Theory of radiative recombination from the metastable excited states of quantum dots

Lucjan Jacak
Institute of Physics, Technical University of Wrocław, Wybrzeże Wyspiańskiego 27, 50-370 Wrocław, Poland

Jurij Krasnyj
Institute of Mathematics, University of Opole, Oleska 48, Opole, Poland

Marek Korkusiński and Arkadiusz Wójs
Institute of Physics, Technical University of Wrocław, Wybrzeże Wyspiańskiego 27, 50-370 Wrocław, Poland

(Received 9 July 1997; revised manuscript received 26 November 1997)

The radiative recombination of an exciton (electron-hole pair) confined in a semiconductor quantum dot is studied within a general model based on the effective-mass approximation. The dependence of the photoluminescence spectrum on the size of the dot and the magnetic field describe well a series of recent experimental results. In particular, a characteristic splitting of the main photoluminescence peak into a doublet or triplet is observed at the critical size and magnetic field, as a consequence of the appearance of metastable states in the exciton spectrum. [S0163-1829(98)06915-X]

I. INTRODUCTION

Recent progress in the semiconductor technology led to the development of various methods for the preparation of quasi-zero-dimensional quantum dots.[1,2] The electron–ion-beam lithography combined with wet or dry etching allowed for a confinement of a well-controlled number of electrons within rectangular or circular dots with diameters of $10-100$ nm.[3] Another method involved the lithographic creation of miniature electrodes above the surface of a quantum well, producing an electric lateral confinement free of edge defects.[4,5] Also reported was a direct growth of so-called self-assembled quantum dots (SAD's), by means of the metal-organic chemical vapor deposition, metal-organic vapor phase epitaxy, or molecular-beam epitaxy, where the dots are spontaneously formed in form of islands of locally increased thickness, due to the high strain present in the deposited layer.[6–11] The SAD's are typically very small, e.g., for $In_xGa_{1-x}As/GaAs$ structures the dot diameter reaches 13 nm,[7] and for InAs/GaAs even 6 nm.[11] The confining barriers can also be created by the focused-laser-beam (FLB)-induced local interdiffusion of atoms between a pair of coupled quantum wells, e.g., in the $GaAs/Al_xGa_{1-x}As$ structure.[12]

A common feature of all quantum dots created by various growth techniques is that they are always in the form of a small islet of a semiconductor material embedded in a surrounding crystal structure of another material, typically in a quantum-well structure. This common property results in a similar behavior of all quantum dots, especially from the point of view of their optical properties. As demonstrated in a series of experiments with various types of dots, the photoluminescence (PL) spectrum probing the recombination of excitons localized in the dots can be characterized by a splitting of the main peak, compared to a single-peak spectrum of the free exciton in a quantum well.[7,12,13] This splitting is sensitive to the diameter of the dot, and is accompanied by a small blueshift.[7,13] In the presence of a magnetic field the additional third peak can be observed,[14] but only at small fields. At strong fields all splittings disappear, and only the main peak in the PL spectrum is observed.

The PL spectrum of a single quantum dot in the absence of a magnetic field was studied by Brunner *et al.*[12] The sample used in the experiment was prepared using the FLB method. The PL measurements were carried out at a temperature of 5 K, and various diameters of the dot. At a large dot size ($\sim$1000 nm) only one PL peak was observed. With the decrease of the dot diameter, the PL maximum exhibited a characteristic splitting and a small blueshift. The maximum splitting (10 meV) occurred for the size of $\sim$450 nm. Below 450 nm the blueshift continued, but the splitting decreased.

The radiative recombination from quantum dots in the presence of a perpendicular magnetic field was recently examined by Bayer *et al.*[14] The $In_xGa_{1-x}As/GaAs$ quantum-dot structures used in the experiment were fabricated using the high-resolution electron-beam lithography. The rearrangement of the PL spectrum was observed under the variation of both the dot diameter and the magnetic field. The maximum number of three resolved transitions were reported in the PL spectrum of dots with the diameter of 35 nm. At zero magnetic field a main line at 1.435 eV and a shoulder at 1.440 eV appeared, and both showed a weak dependence on the magnetic field in the range of low fields ($B \leqslant 2$ T). At $B=4$ T an additional feature appeared at 1.445 eV, and shifted slightly with an increase of the field. At $B=8$ T only the main peak remained. For the 34- and 41-nm dots, at most two PL peaks were observed at lower magnetic fields, and at 8 T the PL spectrum resembled that of the 35-nm dot.

Since the quantum dots seem to offer the possibility of an application in future optical or optoelectronic devices (such as the quantum-dot-based lasers[8,10] or optical memories[15]), an understanding of the optical properties of these systems is needed. A number of papers have already appeared, where this problem was approached using the band structure description of the quantum dot.[16] In this paper we shall explain the observed properties of the PL from quantum dots within

a simple and general model, where the appearance of the higher peaks in the PL spectrum is related to the occurrence of the metastable excited states in the exciton energy spectrum. The model can be applied at least to a qualitative description of various types of quantum dots.

II. MODEL

For the model analysis, we assume that the dot is quasi-two-dimensional (2D), i.e., that it is formed within a narrow quantum well (x-y plane) with an intersubband spacing significantly exceeding the characteristic excitation energies associated with the lateral confinement. The 2D model applies very well to a wide class of quantum dots with the exception of very small pyramidal InAs/GaAs SAD's (typically around $12\times12\times6$ nm).[10,11] However, slightly larger lens-shaped $In_xGa_{1-x}As$/GaAs SAD's (e.g., diameter 36 nm and height 4.4 nm in Ref. 9) can be to a good approximation described by an effective 2D confinement that accounts for their 3D geometry.[16] Further, we assume a rotational symmetry of the lateral confining potential, which is obvious for circular dots, but also well justified in the case of rectangular, electrically defined dots.[17] This holds also for lens-shaped but not for pyramidal SAD's. The assumption of rotational symmetry leads to the conservation of the zth component of total angular momentum of the system, and hence, e.g., to degeneracies in the energy spectrum and to selection rules for optical transitions. If possible deviations from a circular shape (neglected in our model) are not too strong, one can expect that the associated splittings of energy levels are small, and the additional allowed optical transitions have little oscillator strength. The magnetic field is aligned across the quantum-dot plane, i.e., along the z axis (in a 2D model an in-plane component of the field couples only to the electron spin; this can be included by rescaling the Zeeman energy).

As the dot is treated as a small and local perturbation of the crystal field of a surrounding semiconductor, and the interaction between the quantum dot and the carriers has an electric nature, the empty dot attracts the conduction electron and repels the valence hole (or vice versa). However, the hole can be captured by an electron localized in the dot in result of the electron-hole Coulomb attraction. This effect is strongly sensitive to the variation of the dot diameter and the magnetic field, and gives rise to the understanding of the experimentally observed PL phenomena.[7,12–14]

The lateral potential of an empty quantum dot of radius L, which attracts the electron and repels the hole, will be assumed in the Gaussian form: $\mp V_0\ \exp(-r^2/L^2)$, where the signs ''$-$'' and ''$+$'' correspond to the electron and hole, respectively. The Hamiltonian H of the electron-hole pair confined in a quantum dot, and in a perpendicular magnetic field B, written in the effective-mass approach for the simplest two-band semiconductor, contains the single-particle terms H_e and H_h, and the Coulomb interaction potential $V_C(\mathbf{r}_e,\mathbf{r}_h)=-e^2/\epsilon|\mathbf{r}_e-\mathbf{r}_h|$, scaled by the dielectric constant ϵ. The single-electron Hamiltonian is

$$H_e=-\frac{\hbar^2}{2\mu_e}\Delta_e+V_e(r_e)+\frac{1}{2}\hbar\omega_{ce}l_{ze}, \tag{1}$$

where μ_e is the effective mass and $\omega_{ce}=eB/c\mu_e$ is the cyclotron frequency. The single-hole Hamiltonian H_h is obtained from H_e by replacing the subscripts: $e\rightarrow h$, and reversing the sign of the angular-momentum term (due to the opposite charge). We restrict the calculus to the two-band model, including only the heavy-hole subband (the light holes give a weaker contribution to the dot PL spectrum, and the intersubband mixing can often be neglected due to strain, etc.[9]), and hence in the ideal 2D case the effective hole mass is the in-plane heavy-hole mass of a given material. However, in a more realistic case, the effective hole mass could to certain approximation take into account the weak intersubband mixing, actual dimensionality of the dot, and the effects associated with the dot-barrier interface.

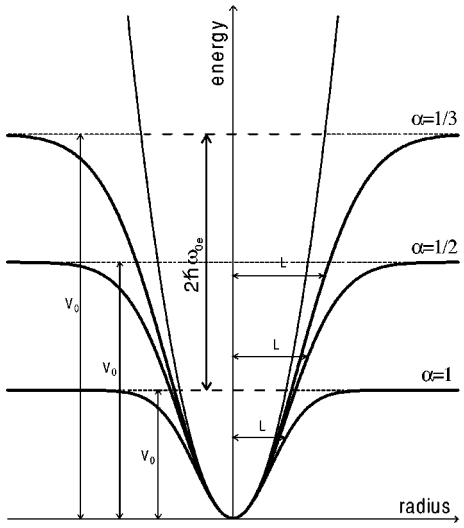

FIG. 1. Schematic picture explaining the physical meaning of parameter $\alpha=\hbar\omega_{0e}/V_0$, controlling the size of a quantum dot; the curvature $\hbar\omega_{0e}$ is fixed.

The bare single-particle potentials in the presence of a magnetic field are

$$V_e(r)=-V_0\ \exp\left(-\frac{r^2}{L^2}\right)+\frac{1}{8}\mu_e\omega_{ce}^2r^2$$
$$=\hbar\omega_{0e}\left[-\frac{1}{\alpha}\exp\left(-\frac{\alpha r^2}{2\lambda_{0e}^2}\right)+\frac{1}{8}\frac{\omega_{ce}^2r^2}{\omega_{0e}^2\lambda_{0e}^2}\right], \tag{2}$$

$$V_h(r)=+V_0\ \exp\left(-\frac{r^2}{L^2}\right)+\frac{1}{8}\mu_h\omega_{ch}^2r^2$$
$$=\hbar\omega_{0e}\left[+\frac{1}{\alpha}\exp\left(-\frac{\alpha r^2}{2\lambda_{0e}^2}\right)+\frac{1}{8}\frac{\omega_{ce}^2r^2}{\omega_{0e}^2\lambda_{0e}^2}\cdot\frac{\mu_e}{\mu_h}\right], \tag{3}$$

where $\omega_{0e}^2=2V_0/\mu_eL^2$, $\lambda_{0e}^2=\hbar/\mu_e\omega_{0e}$, and $\alpha=\hbar\omega_{0e}/V_0=2\lambda_{0e}^2/L^2$.

We will confine our considerations to the case of $V_0/L^2=\text{const}$, i.e., constant curvature of the potential $\omega_{0e}=\text{const}$. This still allows for a variation of the dot diameter, as the parameter α controls the depth of the confining potential V_0 and, connected with it, the radius L. Increase of α corresponds to decrease of the dot dimensions, as shown in Fig. 1.

Within the Hartree approach we will look for the exciton wave functions in the form

$$\Phi(\mathbf{r}_e,\mathbf{r}_h)=\phi_e(\mathbf{r}_e)\phi_h(\mathbf{r}_h), \tag{4}$$

where ϕ_e and ϕ_h are the electron and hole wave functions, satisfying the usual self-consistent equations. The electron and hole Hartree Hamiltonians $\mathcal{H}_e$ and $\mathcal{H}_h$, which include particle-hole interaction, are obtained by adding the self-consistent interaction terms to the single-particle Hamiltonians H_e and H_h (1), i.e., by replacing the single-particle potentials V_e [Eq. (2)] and V_h [Eq. (3)] by the effective Hartree potentials U_e and U_h:

$$U_e(r_e)=V_e(r_e)-\frac{e^2}{\epsilon}\int d\mathbf{r}_h\,\frac{|\phi_h(\mathbf{r}_h)|^2}{|\mathbf{r}_e-\mathbf{r}_h|}, \tag{5}$$

and U_h is obtained from U_e by the interchange of subscripts: $e\leftrightarrow h$. The properties of these potentials are crucial for the PL behavior, because the mutual influence of two carriers located in the dot turns out to be strongly sensitive to the dot diameter and to the external magnetic field. These potentials occur to be generally of double-well shape, what generates the doublets of states for the hole and for the electron, with the same rotational symmetry (zero angular momentum). Products (4) of these single-particle states therefore describe the joint electron-hole-pair (exciton) states, which are metastable against the dipole-type radiative interband transitions (far-infrared).

The electron and hole Hartree energies E_e and E_h (the eigenvalues of $\mathcal{H}_e$ and $\mathcal{H}_h$) are counted from the edges of the conduction and valence bands, respectively. The total energy of the pair (exciton),

$$E=E_e+E_h-\frac{e^2}{\epsilon}\int d\mathbf{r}_e\int d\mathbf{r}_h\,\frac{|\phi_e^*(\mathbf{r}_e)|^2|\phi_h^*(\mathbf{r}_h)|^2}{|\mathbf{r}_e-\mathbf{r}_h|}, \tag{6}$$

is thus counted from the band gap E_g.

III. ELECTRON-HOLE-PAIR STATES IN THE QUANTUM DOT

Provided that

$$\frac{e^2}{\epsilon}\int d\mathbf{r}_h\,\frac{|\phi_h(\mathbf{r}_h)|^2}{|\mathbf{r}_e-\mathbf{r}_h|}<\frac{e^2}{\epsilon L}<\hbar\omega_{0e}, \tag{7}$$

where $\hbar\omega_{0e}$ is of the order of the single-electron excitation energy in the dot, we can use perturbation methods to solve the Hartree equations defined by $\mathcal{H}_e$ and $\mathcal{H}_h$. In the case of the commonly used material GaAs, the right-hand relation means $L>20$ nm for $\hbar\omega_{0e}=5$ meV (or $L>2$ nm for $\hbar\omega_{0e}=50$ meV), and holds.

In the zeroth-order approximation, in Eq. (5) we neglect the electron-hole interaction and thus find the eigenfunctions ϕ_e and eigenenergies E_e of the single-electron Hamiltonian H_e. The low-energy electron wave functions are localized in the region of $r\sim\lambda_{0e}$. Thus, in order to find the electron ground state, we can expand V_e in the power series with respect to the dimensionless parameter $\lambda_{0e}/L<1$ (e.g., for GaAs, $\lambda_{0e}\sim 15$ nm for $\hbar\omega_{0e}\sim 5$ meV):

$$V_e(r)\approx -V_0+\tfrac{1}{2}\mu_e\tilde{\omega}_{ce}^2 r^2, \tag{8}$$

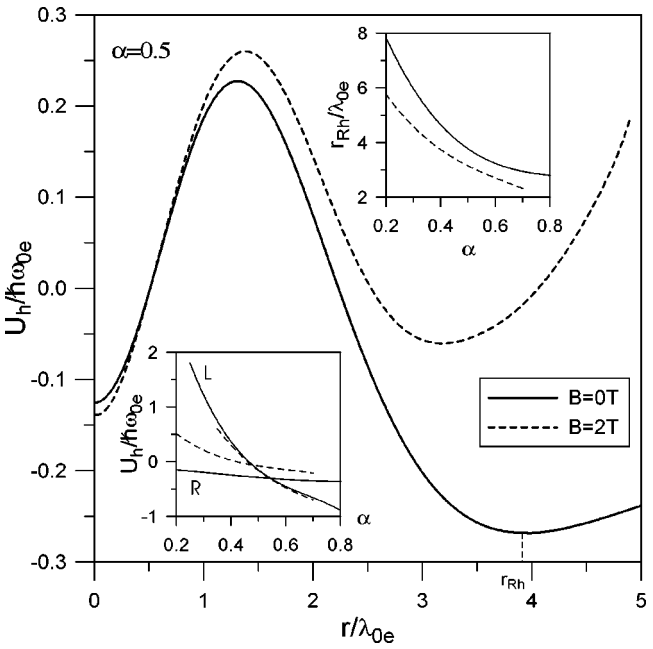

FIG. 2. Typical shape of the hole Hartree potential U_h at $B=0$ (solid line) and at a magnetic field $B=2$ T (dashed line), for the size parameter $\alpha=0.5$. Insets show the minimum values of U_h, U_{Lh}, and U_{Rh}, and the position of the second minimum, r_{Rh}, as a function of the size parameter α.

where $\tilde{\omega}_{ce}^2=\omega_{0e}^2+\omega_{ce}^2/4\equiv\omega_{0e}^2\beta^2$. In this approximation, the ground-state energy and wave function have the form

$$E_e=-V_0+\hbar\tilde{\omega}_{ce}=\hbar\omega_{0e}\left(-\frac{1}{\alpha}+\beta\right), \tag{9}$$

$$\phi_e(\mathbf{r})=\frac{1}{\sqrt{\pi}\lambda_e}\exp\left(-\frac{r^2}{2\lambda_e^2}\right), \tag{10}$$

where $\lambda_e^2=\hbar/\mu_e\tilde{\omega}_{ce}=\lambda_{0e}^2/\beta$. We can restrict our considerations to the interval $1\geq\beta^{-1}\geq\alpha\geq 0$, so as to avoid the artifact of our approach ($E>0$, i.e., the electron is not confined in the dot). In the absence of a magnetic field ($B=0$), we have $\beta=1$, and therefore the above condition simplifies to $1\geq\alpha\geq 0$.

In the next step of the perturbation, we put the zeroth-order electron wave function (10) into the hole Hartree potential [cf. Eq. (5)], and arrive at the eigenequation for the hole Hartree Hamiltonian $\mathcal{H}_h$, with the potential U_h, reading

$$U_h(r)=V_0\exp\left(-\frac{r^2}{L^2}\right)+\frac{1}{8}\frac{\mu_e^2}{\mu_h}\omega_{ce}^2 r^2-\frac{e^2}{2\lambda_{0e}^2}\sqrt{\pi\beta}\times\exp\left(-\frac{\beta r^2}{2\lambda_{0e}^2}\right)I_0\left(-\frac{\beta r^2}{2\lambda_{0e}^2}\right), \tag{11}$$

where I_0 is the Bessel function.

From Eq. (11) it follows that the effective potential of the hole U_h has two minima in the absence of a magnetic field (the positions of these minima will be denoted as $r_{Lh}=0$ and $r_{Rh}>0$), and decays to zero for $r\to\infty$. The subscripts L and R denote the left (central) and right (outer) minima of the

profile of this potential, respectively (cf. solid line in Fig. 2 for $\alpha=0.5$). With the increase of the parameter α (corresponding to a decrease of dot dimension), the energies of the pair of minima, $U_{Lh}=U_h(0)$ and $U_{Rh}=U_h(r_{Rh})$, decrease. Simultaneously, the second minimum approaches the first one, and disappears for a large enough α, i.e., a small enough quantum dot ($\alpha\sim 0.8$). For the calculations, we used parameters appropriate for the GaAs quantum well, and the quantum dot with the curvature of confinement $\hbar\omega_{0e}=7.5$ meV.

In the presence of a magnetic field the potential U_h also has two minima, but it tends to infinity for $r\to\infty$, as a result of the enhancement of the hole confinement due to the magnetic field (cf. dashed line in Fig. 2, for $\alpha=0.5$ and $B=2$ T; see also Fig. 7). The minima U_{Lh} and U_{Rh} decrease with an increase of α, and the second minimum approaches the first one (i.e., r_{Rh} decreases) and disappears for large enough α ($\alpha\sim 0.8$). At a fixed α the potential U_{Lh} does not change significantly with an increase of the magnetic field, but U_{Rh} grows rapidly. At high fields the second minimum disappears. The behavior of the hole potential is illustrated in the insets of Figs. 2 and 7, where all features described above are clearly visible.

It is important to notice that the appearance of a pair of wells in the effective binding potential of a hole (and further also of an electron) is caused by the nonsingularity of the bare lateral potential, combined with the singularity of the electron-hole Coulomb interaction. This leads to a local minimum in the hole Hartree potential around the position of the electron, even if it coincides with the local maximum of the bare lateral potential of the dot. Actually, due to the finite thickness of the well and the spread of the electron and hole wave functions across the dot, the effective Coulomb potential as a function of the in-plane distance is not singular. However, for a narrow well it has a sharp minimum around $|\mathbf{r}_e-\mathbf{r}_h|=0$, and our arguments still hold. Note that calculations performed for magnetoexcitons in a quantum well trapped by donors or acceptors, where the bare confinement has the atomiclike singularity, reveal the absence of a double-well effective Hartree potential structure, and in that case no metastable states appear. This has also been confirmed experimentally.[18]

Taking the advantage of the double-well structure of the potential U_h, we can solve the hole motion by independently studying the motions in the two wells, and later including the coupling between the wells via the off-diagonal tunneling matrix element. Thus the pair of lowest-energy hole states will be approximated by diagonalizing the Hamiltonian $\mathcal{H}_h$ in the subspace spanned by the pair of ground states in the two wells treated separately: ψ_{Lh} and ψ_{Rh}, with the energies E_{Lh} and E_{Rh}, respectively. The ground state ($i=1$) and the first excited state ($i=2$) of the hole are hence assumed in the form

$$\phi_h^{(i)}(\mathbf{r})=c_L^{(i)}\psi_{Lh}(\mathbf{r})+c_R^{(i)}\psi_{Rh}(\mathbf{r}), \tag{12}$$

with the coefficients c_L and c_R calculated from the minimum-energy condition. Due to the nonvanishing coupling between the wells, the corresponding pair of energies $E_h^{(1)}$ and $E_h^{(2)}$ are always separated by a gap, even in the case of degeneracy of the single-well levels ($E_{Lh}=E_{Rh}$). The details of the calculation are presented in Appendix A, and here

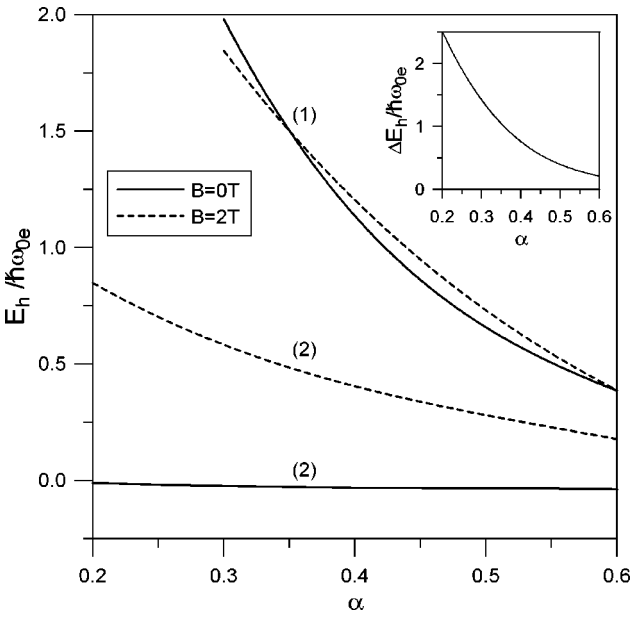

FIG. 3. Hole Hartree energies $E_h^{(1)}$ (hole in the dot center) and $E_h^{(2)}$ (hole on a ring around the dot center) at magnetic fields $B=0$ (solid line) and $B=2$ T (dashed line), as a function of the size parameter α. The inset shows the difference between the energy levels in the absence of a magnetic field.

let us notice that due to the same parity (zero angular momentum) of both single-well ground states ψ_{Lh} and ψ_{Rh}, the two coupled states $\phi_h^{(1)}$ and $\phi_h^{(2)}$ are also of the same parity. Summarizing, as a result of a double-well structure of the Hartree potential, the low-lying excited state appears in the hole energy spectrum with zero angular momentum, similar to what occurs in the ground state. Hence we deal with a doublet of hole states with a forbidden dipole radiative transition.

In the absence of a magnetic field the energy $E_h^{(1)}$ is positive and the energy $E_h^{(2)}$ is negative (cf. solid lines in Fig. 3). This means that the state with $i=1$ does not describe a hole localized in the quantum dot, and the hole is localized only in the state with $i=2$. The coefficient $|c_L^{(2)}|$ increases with the increase of α, but always remains smaller than $|c_R^{(2)}|$ (cf. Appendix A), i.e., the hole in the state with $i=2$ is localized on the ring around the second minimum of the potential U_h.

The inclusion of a magnetic field increases the confinement of the hole [$U_h(r)\to\infty$ for $r\to\infty$], which is now localized in the dot in both states with $i=1$ and 2. The hole in the state with $i=1$ is localized in the center of the dot around the first minimum of the potential U_h ($|c_L^{(1)}|>|c_R^{(1)}|$), while in the state with $i=2$ it is localized on the ring around the second minimum ($|c_L^{(2)}|<|c_R^{(2)}|$). At a fixed magnetic field, when α increases (i.e., the dot diameter decreases), the values of $E_h^{(1)}$ and $E_h^{(2)}$, and the difference between them $\Delta E=|E_h^{(1)}-E_h^{(2)}|$, decrease (cf. dashed lines in Fig. 3, for $B=2$ T). When the second minimum disappears (for $\alpha\sim 0.75$), the energy levels meet. At a fixed α, with the increase of the magnetic field, the energy $E_h^{(1)}$ changes only slightly, but $E_h^{(2)}$ rapidly increases. If the field is sufficiently strong, the energy levels meet when the second minimum disappears (e.g., for $\alpha=0.3$ the levels meet at $B\sim 5$ T).

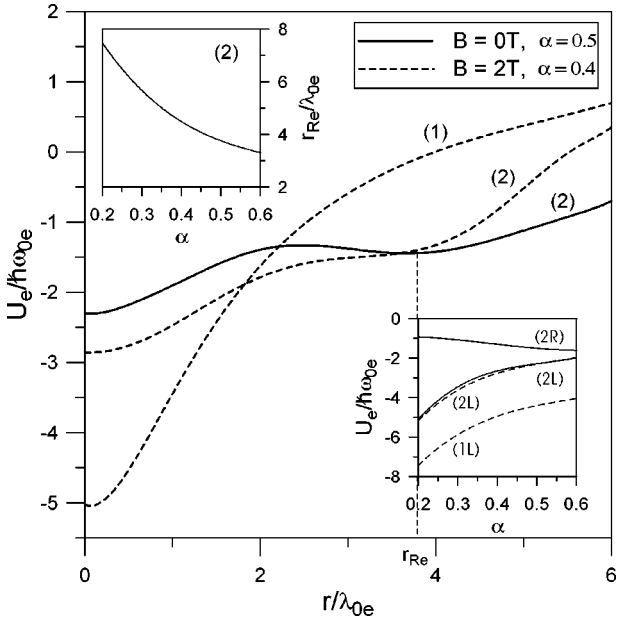

FIG. 4. Typical shape of the electron Hartree potential $U_e^{(2)}$ (hole on a ring around the dot center) at a magnetic field $B=0$ (solid line, size parameter $\alpha=0.5$) and of the potentials $U_e^{(1)}$ and $U_e^{(2)}$ (hole in the dot center and on a ring around the dot center, respectively) for $B=2$ T (dashed lines, $\alpha=0.4$). Insets show the minimum values of these potentials—both minima of $U_e^{(2)}$ at $B=0$, and the first (left) minima of $U_e^{(1)}$ and $U_e^{(2)}$ at $B=2$ T (bottom right), and the position of the second (right) minimum at $B=0$ (top left), as functions of the size parameter α.

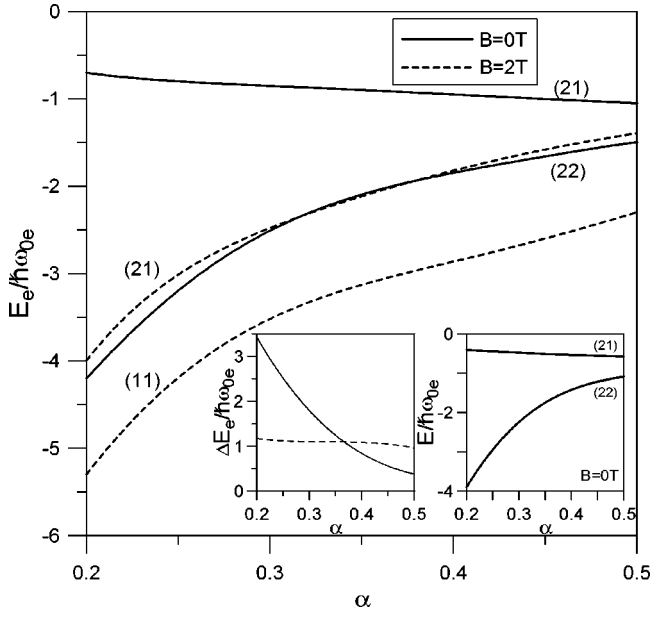

FIG. 5. Electron Hartree energies E_e as a function of the size parameter α. Solid line: magnetic field $B=0$, the bound states are $E_e^{(21)}$ and $E_e^{(22)}$ (hole on a ring around the dot center; electron in the dot center and on a ring around the dot center, i.e., on top of the hole, respectively). Dashed line: magnetic field $B=2$ T; the bound states are $E_e^{(21)}$ and $E_e^{(11)}$ (electron in the dot center; hole on a ring around the dot center and in the dot center, i.e., on top of the electron, respectively). Insets: the distance between the energy levels for $B=0$ and 2 T (left). $E^{(22)}$ and $E^{(21)}$: Exciton recombination energies in the absence of a magnetic field (hole on a ring around the dot center, electron in the dot center and on a ring around the dot center, i.e., on top of the hole, respectively), as a function of the size parameter α (right).

After having calculated the energies and wave functions of the ground ($i=1$) and the first excited ($i=2$) states of the hole, we shall now proceed with the perturbation calculus, and find for these states the pair of Hartree potentials $U_e^{(1)}$ and $U_e^{(2)}$ acting on the electron [cf. Eq. (5)]. A brief description of this procedure is presented in Appendix B.

In the absence of a magnetic field, the hole is localized only for $i=2$, and in this case we consider only the function $U_e^{(2)}$, which decays to zero for infinite radii. The potential $U_e^{(2)}$ usually also has two minima, the positions of which we denote as $r_{Le}^{(2)}=0$ and $r_{Re}^{(2)}>0$. The characteristic shape of this curve is presented in Fig. 4, for $\alpha=0.5$ (solid line), and in Fig. 7(b). When the parameter α increases, the minimum value $U_{Le}^{(2)}\equiv U_e^{(2)}(0)$ increases, and decrease both $U_{Re}^{(2)}\equiv U_e^{(2)}(r_{Re}^{(2)})$ and the distance between the minima $r_{Re}^{(2)}$ (equal roughly to $r_{Rh}^{(2)}$).

In the presence of a magnetic field, it is necessary to consider both functions $U_e^{(1)}$ and $U_e^{(2)}$, which rise to infinity for infinite radii. The potentials $U_e^{(1)}$ and $U_e^{(2)}$ usually have a single minimum at $r=0$ (cf. dashed lines in Fig. 4). Only for specific values of α and B can the function $U_e^{(2)}$ have a pair of minima (e.g., for $\alpha=0.5$ and $B=4$ T). Here, at a fixed magnetic field, the minimum values of functions U_e increase as α increases (cf. the inset in Fig. 4 for $B=2$ T and Fig. 7).

After a discussion of the properties of potentials U_e, we shall put these functions into the electron Hartree Hamiltonian $\mathcal{H}_e$ and solve the corresponding Schrödinger equation. Since again, in general, we are dealing with a double-well structure of the Hartree potential U_e, the two lowest energies and corresponding wave functions can be calculated analogously as in the case of the hole (cf. Appendix A). Whenever $U_e^{(i)}$ has two minima, there will be two low-energy states with the same parity (zero angular momentum) in the electron energy spectrum, denoted as $\phi_e^{(ij)}$ ($j=1$, 2 indicates the electron state and i indicates the hole state). These states are approximated in the form of linear combinations of the ground states of the two uncoupled wells,

$$\phi_e^{(ij)}(\mathbf{r})=d_L^{(ij)}\psi_{Le}^{(i)}(\mathbf{r})+d_R^{(ij)}\psi_{Re}^{(i)}(\mathbf{r}). \tag{13}$$

The state with $j=1$ describes the electron localized in the center of the dot ($|d_L^{(i1)}|>|d_R^{(i1)}|$), and the state with $j=2$ describes the electron localized on the ring around the second minimum of the potential U_e ($|d_L^{(i2)}|<|d_R^{(i2)}|$). Summarizing, depending on whether $U_e^{(i)}$ has one or two minima, there will or will not be a low-energy excited electron state with the same parity as the ground state.

Detailed calculations show that at zero and very weak magnetic fields, when the hole occupies the state with $i=2$ (energy $E_h^{(2)}$), the electron can occupy each of the two states with $j=1$ and 2 (energies $E_e^{(21)}$ and $E_e^{(22)}$). As shown in Fig. 5, when α increases, $E_e^{(21)}$ increases and $E_e^{(22)}$ decreases. The distance between the electron energy levels, $\Delta E=|E_e^{(22)}-E_e^{(21)}|$, initially decreases, and then reaches its minimum value at $\alpha\sim 0.5$ and increases again.

In relatively weak magnetic fields ($B\sim 2-3$ T), each of the two hole states with $i=1$ and 2 (energies $E_h^{(1)}$ and $E_h^{(2)}$) corresponds to the appropriate electron state with $j=1$ (energy $E_e^{(11)}$ or $E_e^{(21)}$, respectively). With the increase of α, the energies $E_e^{(11)}$ and $E_e^{(21)}$ increase, while the distance between them $\Delta E=|E_e^{(21)}-E_e^{(11)}|$ decreases. For α large enough ($\alpha\sim 0.6$), the second minimum of the hole potential disappears, and the levels $E_e^{(11)}$ and $E_e^{(21)}$ meet (cf. Fig. 5 for $B=2$ T).

An interesting feature which occurs in higher magnetic fields ($B\sim 4-6$ T) is that, in a certain range of parameter α (dot size), when the hole occupies a state with $i=2$, the electron can be in each of the two states with $j=1$ and 2 (energies $E_e^{(21)}$ and $E_e^{(22)}$). When the magnetic field increases at a fixed α, the electron energies $E_e^{(11)}$ and $E_e^{(21)}$ increase, grow closer to each other, and finally meet when the field exceeds the critical value. For α both too small and too large, the second minimum of the electron potential $U_e^{(2)}$ disappears, and only one electron state with $j=1$ (energy $E_e^{(21)}$) corresponds to the hole state with $i=2$.

Let us now turn to a description of joint electron-hole pair states. As shown above, the number of these states, with low total energy and zero electron and hole angular momenta, is determined by the number and depths of minima in the electron and hole Hartree potentials U_h and U_e, which significantly depend on the dot size and magnetic field. The dependencies of U_h and $U_e^{(2)}$ have been plotted in the form of 3D graphs in Fig. 7 (potential $U_e^{(1)}$ always has only one minimum at $r=0$, and has not been shown). Combining the electron and hole states together, we can classify the possible states of the electron-hole pair ($i,j=1,2$)

$$\Phi^{(ij)}(\mathbf{r}_h,\mathbf{r}_e)=\phi_h^{(i)}(\mathbf{r}_h)\phi_e^{(ij)}(\mathbf{r}_e), \tag{14}$$

with energies

$$E^{(ij)}=E_h^{(i)}+E_e^{(ij)}+V_C^{(i)}. \tag{15}$$

In the above, $V_C^{(i)}$ stands for the Coulomb energy of the pair [Eq. (6)], approximated by the expectation value of the Coulomb potential V_C in the exciton state, where the hole occupies the state i, and the electron is in its zeroth-order state given by formula (10). In this approximation the interaction energy can be evaluated analytically [cf. expression (A29)].

Out of four possible joint states $\Phi^{(ij)}$, the state $\Phi^{(12)}$ is never stable or metastable, as none of the particles occupies a local minimum of its Hartree potential. The other three, $\Phi^{(11)}$, $\Phi^{(22)}$, and $\Phi^{(21)}$, can be stable or metastable, depending on the dot size and the magnetic field (which govern their energies with respect to the continuum of unbound electron-hole states). In $\Phi^{(11)}$ and $\Phi^{(22)}$, the electron and hole, roughly speaking, sit on top of each other. In $\Phi^{(21)}$, the electron and hole are spatially separated, but both occupy local minima of their Hartree potentials (electron in the minimum of its bare lateral potential and hole away from the maximum of its bare lateral potential).

The crucial property of states (14) is that the corresponding electron and hole Hartree states are all of the same parity (all have zero angular momentum), and therefore the dipole-type radiative transitions between each pair of levels are forbidden. Hence, when the phonon-assisted relaxation processes are suppressed due to the small dot dimensions,[13] and the only efficient relaxation mechanism involves the emission of a far-infrared photon, the excited states (14) are *metastable*. Unlike all other excited states, the metastable states make traps for confined excitons, and lead to the appearance of additional, higher-energy peaks in the PL spectra of quantum dots. This property is crucial for our model, and results from the double-well structure of the effective electron and hole potentials. Splittings of the electron and hole energy levels gives rise to the explanation of the splittings of the PL spectra. At this point our approach differs from the simple model of the single well, described, e.g., by Raymond *et al.*[9] Note that a splitting of the PL peak is observed even at a very low excitation power [cf. Fig. 6(c)],[12] which strongly supports the explanation in terms of metastable states.

Since the energy $E^{(ij)}$ is counted from the band gap, the actual annihilation energy of the electron-hole pair in the state (ij) is $\hbar\omega^{(ij)}=E_g+E^{(ij)}$, while the distance between the two PL peaks reads

$$\Delta E^{(ij,i'j')}=|E^{(ij)}-E^{(i'j')}|. \tag{16}$$

Following the earlier discussion of the stability of electron and hole states depending on the magnetic field and the dot radius, we can predict the following structure of the PL spectra.

In zero or very weak magnetic fields, there are two electron-hole pair states with $(ij)=(21)$ and (22), and thus there are two PL peaks separated by $\Delta E^{(21,22)}=|E_e^{(22)}-E_e^{(21)}|$. The dependence of the spectrum on the dot size is shown in Fig. 6, where the experimental data are included for comparison. The intensities of peaks were evaluated from the overlap of electron and hole wave functions. With an increase of α, the ground-state energy E_{21} increases, i.e., the main PL peak shifts toward higher energies, which has been verified by numerous experiments. The distance between the main and additional PL peaks $\Delta E^{(21,22)}$ at first decreases, and then reaches its minimum value and increases. At the critical α, when the distance between the peaks reaches minimum (this critical α depends on $\hbar\omega_{0e}$), the two peaks have similar intensities, while for smaller and larger dots the main peak dominates. This is exactly what has been observed in experiment.[12]

In relatively weak magnetic fields ($B\sim 2-3$ T), there are two electron-hole pair states with $(ij)=(11)$ and (21), and thus there are two PL peaks separated by $\Delta E^{(11,21)}=|E_h^{(11)}-E_e^{(21)}+V_C^{(1)}-V_C^{(2)}|$. With the increase of α, the energies E_{11} and E_{21} increase (i.e., both main and additional PL peaks shift toward higher energies), while the distance between them at first changes only slightly, and then rapidly decreases. Above the critical value of α the energies E_{11} and E_{21} meet.

In moderate magnetic fields ($B\sim 4-6$ T), and for a certain range of the parameter α, in addition to the doublet of states with $(ij)=(11)$ and (21), the third electron-hole pair state appears with $(ij)=(22)$. Thus the third PL peak emerges, separated from the second by $\Delta E^{(21,22)}=|E_e^{(22)}-E_e^{(21)}|$. When α is either too small or too large, the triplet of peaks is replaced by a doublet, and further by a single peak for very small dots. Note that three is

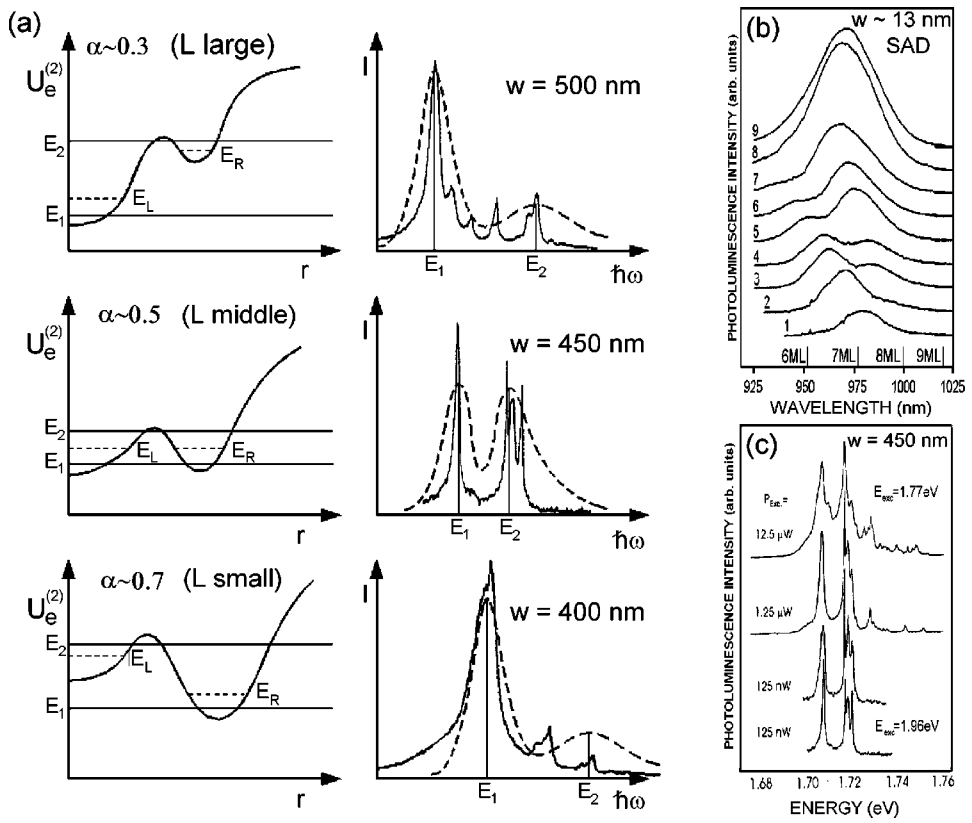

FIG. 6. (a) Left: electron Hartree potentials $U_e^{(2)}$ (hole on a ring around the dot center) for three different sizes of the quantum dot, in the absence of the magnetic field. Right: corresponding PL spectra; dashed lines—peak intensities calculated from the electron-hole overlap for $\alpha=0.3$, 0.5, and 0.7; solid lines—experimental PL spectra after Ref. 12 (single $GaAs/Al_xGa_{1-x}As$ interlayer-diffused dot of diameter w). (b) PL spectrum of an $In_xGa_{1-x}As/GaAs$ SAD with diameter $\sim$13 nm; numbers 1–9 label spectra corresponding to different average dot sizes obtained with selective excitation, after Ref. 7. (c) PL spectra of a quantum dot with diameter 450 nm for various excitation powers, after Ref. 12.

the maximum number of metastable states of a single exciton predicted within our model at any magnetic field and dot size, which agrees with the experiment of Bayer *et al.*[14] In strong fields ($B\geqslant 8$ T) higher peaks subsequently disappear, and the PL spectrum consists of a single main peak, which is also verified experimentally.[14]

Summarizing, depending on the size of the quantum dot, two types of a magnetic-field evolution of the PL spectrum are possible: (i) Medium dot: there are two peaks at $B_0=0$, the third one emerges at $B_1>0$ and disappears at $B_2>B_1$, and finally the second peak disappears at $B_3>B_2$. (ii) Small or large dot: there are two peaks for all fields below the critical value, at which the higher peak disappears. The predicted behavior has been confirmed by experiment—cf. bottom-right inset in Fig. 7.

IV. CONCLUSION

In conclusion, the PL spectrum, due to recombination of the exciton captured by the quantum dot, has been studied theoretically both in the absence and presence of a magnetic field. The electron and hole effective potentials, determined in the effective-mass approach, exhibit a double-well structure, which is a consequence of the nonsingularity of the bare lateral electron and hole potentials. The positions and depths of the pair of minima of these potentials depend strongly on the dot diameter. This results in a blueshift of the overall PL spectrum with a diminishing of the dot, and the splitting of the PL peak. This splitting is due to the existence of a doublet of excitonic states, in which both electron and hole have zero angular momentum, and hence the dipole-type far-infrared (FIR) transitions between these states are forbidden. Let us underline that the simple band-model description of the dot does not allow for such an effect. Moreover, the splitting observed experimentally does not change even at a very small excitation power,[12] which supports the idea of metastable states.

Inclusion of a magnetic field modifies electron and hole confinements, and has a significant influence on the shape of the effective potentials. In weak magnetic fields the hole potential has the shape of the double well, but both corresponding electron potentials have only a single minimum. Therefore, the two PL peaks are observed. For intermediate magnetic fields and for a certain size of the dot, an additional minimum appears in the electron potential, leading to the appearance of an additional, third PL peak. In strong magnetic fields both potentials have a single-well structure due to the enhancement of the confinement for both carriers. It reduces the PL spectrum to a single peak. The presented behavior of the quantum dot PL spectrum agrees very well with the available experimental data.[7,12–14]

Let us also state that the behavior described above allows for an understanding of the structure of the PL spectrum of

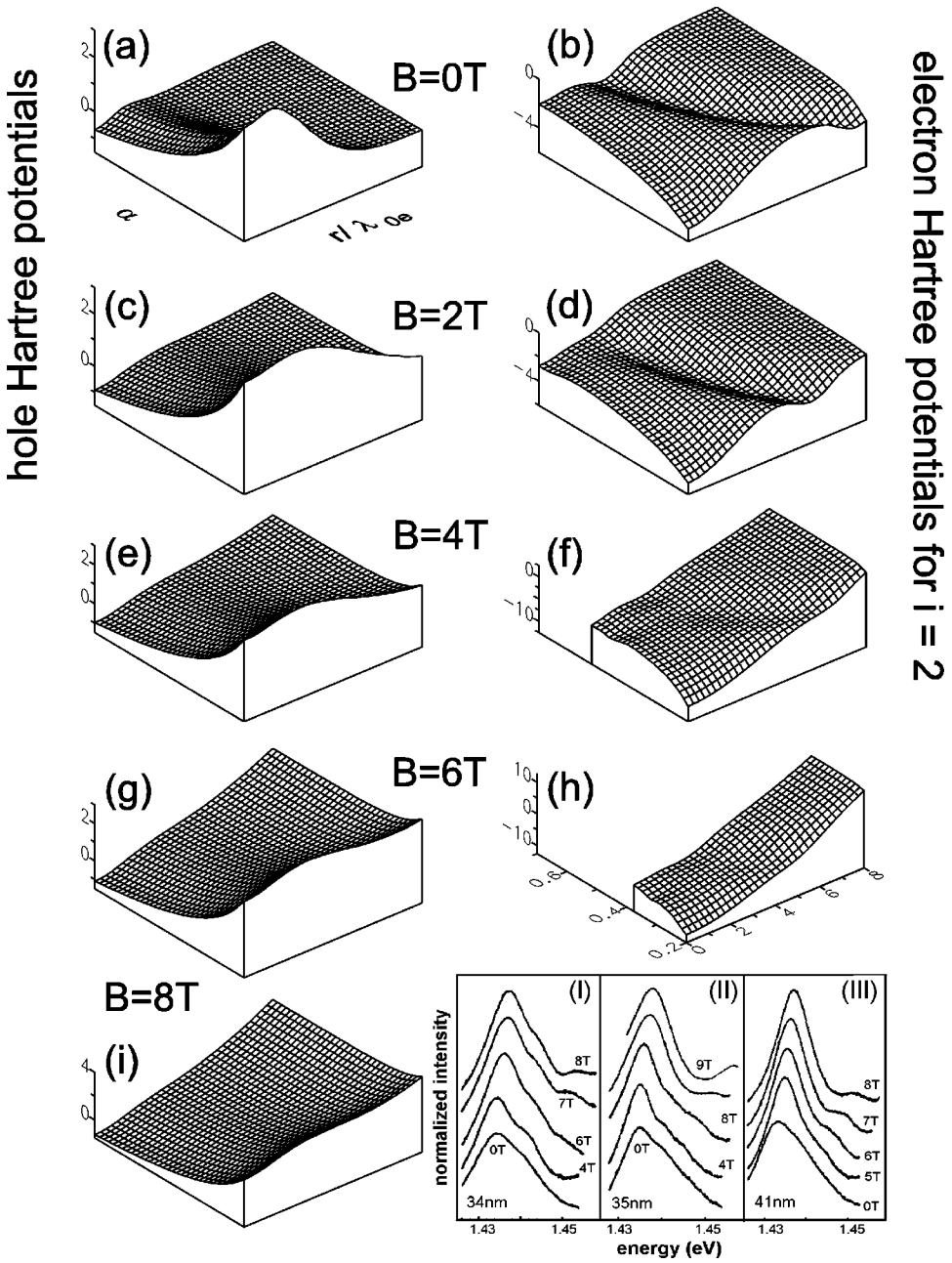

FIG. 7. Dependence of the hole (left) and electron (right) Hartree potentials (U_h and $U_e^{(2)}$) on the size parameter α for the magnetic fields $B=0$, 2, 4, 6, and 8 T. Potentials in vertical axes are given in the units of $\hbar\omega_{0e}$, and the horizontal axes are common for all graphs. At $B=4$ and 6 T the bound hole state with $i=2$ exists only below the critical value of α, and at $B=8$ T does not exist in the entire shown range $\alpha=0.2-0.7$. Inset: the experimental PL spectra, after Ref. 14; the measurements were carried out on $In_xGa_{1-x}As/GaAs$ dots with diameters 34 nm (I), 35 nm (II), and 41 nm (III), and in magnetic fields 0–9 T.

highly excited dots, when more than one exciton is captured. Recent experiments on highly excited lens-shaped $In_xGa_{1-x}As/GaAs$ SAD's (Ref. 9) reveal the existence of three peaks without the magnetic field, which split into four in the presence of a magnetic field. The third peak was also observed for highly excited dots created by the interdiffusion method [cf. Fig. 6(c)].[12] A qualitative explanation of this phenomenon is based on the existence of the singlet and triplet states of an electron pair in the many-exciton complex (it is crucial to consider a two-electron–one-hole or a two-hole–one-electron complex). These states also have zero angular momentum, which leads to the metastability against the FIR dipole transition, and give rise to four peaks in the PL spectrum. However, the appropriate exchange term is very small (for GaAs), and two of these four states are almost degenerate, but this degeneracy is removed by the magnetic field. It mimics the experimental behavior mentioned above. For pyramidal InAs/GaAs SAD's the theoretical approach should account for the lack of the rotational symmetry of the lateral potential. It may result in the appearance of allowed transitions, and thus in the modification of the PL spectrum. However, if the nonrotational correction is small, additional transitions are expected to have small oscillator strength. Therefore, compared to our model, we may expect qualita-

tively similar PL spectrum, with broadened or fine-shaped maxima. It has been observed in experiments.[11]

ACKNOWLEDGMENTS

This work was supported by KBN Grant No. PB 674/P03/96/10. A. Wójs also acknowledges financial support from the Foundation for Polish Science.

APPENDIX A

We consider a particle (hole) moving in an axially symmetric, double-well potential U_h, and subject to a magnetic field. Around each minimum, the potential U_h can be expanded into a power series of radius r, and in the proximity of each minimum we can use the quadratic approximation. Thus, around the first minimum at $r_{Lh}=0$, we have

$$U_h(r)\approx U_{Lh}+\tfrac{1}{2}\mu_h\omega_{Lh}^2 r^2, \tag{A1}$$

where the minimum value is $U_{Lh}=U_h(0)$, and the curvature around the minimum is given by a characteristic frequency ω_{Lh}, defined as $\mu_h\omega_{Lh}^2=U_h''(0)$. The ground-state wave function and energy of a hole moving in such a single quadratic well are

$$\psi_{Lh}(\mathbf{r})=A_{Lh}\,\exp\left[-\frac{1}{2}\left(\sigma_L\frac{r}{\lambda_{0e}}\right)^2\right], \tag{A2}$$

$$E_{Lh}=U_{Lh}+\hbar\omega_{Lh}, \tag{A3}$$

where $\sigma_L^2=\mu_h\omega_{Lh}^2/\mu_e\omega_{0e}^2$ and $A_{Lh}=\sigma_L/\sqrt{\pi}\lambda_{0e}$.

In the proximity of the second minimum at $r_{Rh}>0$, the potential U_h is approximated as

$$U_h(r)\approx U_{Rh}+\tfrac{1}{2}\mu_h\omega_{Rh}^2(r-r_{Rh})^2, \tag{A4}$$

where the minimum value is $U_{Rh}=U_h(r_{Rh})$, and the curvature is defined as $\mu_h\omega_{Rh}^2=U_h''(r_{Rh})$. The ground-state wave function of a hole in this potential will be assumed in the following form:

$$\psi_{Rh}(\mathbf{r})=A_{Rh}\,\exp\left[-\frac{1}{2}\left(\sigma_R\frac{r-r_{Rh}}{\lambda_{0e}}\right)^2+f_h\left(\sigma_R\frac{r}{\lambda_{0e}}\right)\right], \tag{A5}$$

where $\sigma_R^2=\mu_h\omega_{Rh}^2/\mu_e\omega_{0e}^2$. Note, that both ψ_{Lh} and ψ_{Rh} have the same parity (zero angular momentum). The function f_h can be calculated by putting the above wave function into the Schrödinger equation, what leads to the following differential equation:

$$-f_h''(z)+2\,f_h'(z)(z-z_{Rh})+[f_h'(z)]^2 - \frac{f_h'(z)}{z}+\frac{z_{Rh}}{z}-2+2\,\frac{E_{Rh}-U_{Rh}}{\hbar\omega_{0e}}=0, \tag{A6}$$

where $z=\sigma_R r/\lambda_{0e}$ and $z_{Rh}=\sigma_R r_{Rh}/\lambda_{0e}$. In the limit of $z\to\infty$, we expand the solution f_h into the series

$$f_h(z)=\sum_{n=1}^{\infty} a_n(z_{Rh}/z)^n, \tag{A7}$$

and in the limit of $z\to 0$, into

$$f_h(z)=\sum_{n=1}^{\infty} b_n(z_{Rh}\cdot z)^n. \tag{A8}$$

By substituting the above into Eq. (A6), the series of coefficients a and b can be calculated up to a desired order, namely, $\{a\}=\frac{1}{2},\frac{1}{4},\frac{1}{6}-1/12z_{Rh}^2,\ldots$, and $\{b\}=1,-\frac{1}{2},2/9z_{Rh}^2,\ldots$. Since the series of $|a_n|$ and $|b_n|$ are decreasing, the asymptotic expansions for f_h in both limits of $z\to 0$ and ∞ can be obtained by keeping a fixed number of N terms in Eqs. (A7) or (A8), respectively. The approximate expression valid in the entire range of z can be constructed, e.g., by adding the $(N+1)$-order term to one of the limiting expansions, with the coefficient calculated from the continuity condition. The eigenenergy associated with the wavefunction ψ_{Rh} [cf. Eq. (A5)] is

$$E_{Rh}=U_{Rh}+\hbar\omega_{Rh}, \tag{A9}$$

and the constant A_{Rh} is found from the normalization condition

$$A_{Rh}\approx\frac{\sigma_R}{\sqrt{2\pi}\lambda_{0e}}\exp[f_h(z_{Rh})] \times\left\{\frac{1}{2}\exp[-z_{Rh}^2]+\frac{\sqrt{\pi}}{2}z_{Rh}[1+\Phi(z_{Rh})]\right\}^{-1/2}, \tag{A10}$$

where

$$\Phi(z_{Rh})=\frac{2}{\sqrt{\pi}}\int_0^{z_{Rh}}dz\,\exp(-z^2) \tag{A11}$$

is the error integral.

In the next step, the coupling between the two wells of the potential U_h is introduced via the tunneling matrix element, leading to the mixing of the two states ψ_{Lh} and ψ_{Rh}. The coefficients c_L and c_R in Eq. (12) are calculated from the minimum-energy condition in the ground state $\phi_h^{(1)}$, and the orthogonality of two states: $\phi_h^{(1)}\perp\phi_h^{(2)}$. The energy of the hole in the state with given c_L and c_R reads

$$E_h=c_L^2\int d\mathbf{r}\;\psi_{Lh}(\mathbf{r})\mathcal{H}_h\psi_{Lh}(\mathbf{r})+c_R^2\int d\mathbf{r}\;\psi_{Rh}(\mathbf{r})\mathcal{H}_h\psi_{Rh}(\mathbf{r}) +2c_Lc_R\int d\mathbf{r}\;\psi_{Lh}(\mathbf{r})\mathcal{H}_h\psi_{Rh}(\mathbf{r}). \tag{A12}$$

The condition for the vanishing of the variations of E_h with respect to c_L and c_R can be conveniently written using the coefficients c_L^* and c_R^*, defined as

$$\begin{bmatrix}c_L\\c_R\end{bmatrix}=\frac{1}{1-\rho_h^2}\begin{bmatrix}1&-\rho_h\\-\rho_h&1\end{bmatrix}\begin{bmatrix}c_L^*\\c_R^*\end{bmatrix}, \tag{A13}$$

where ρ_h stands for the overlap integral:

$$\rho_h=\int d\mathbf{r}\;\psi_{Lh}(\mathbf{r})\psi_{Rh}(\mathbf{r}). \tag{A14}$$

In terms of c_L^* and c_R^*, the minimum-energy condition has the form of the following eigenequation:

$$\begin{bmatrix}E_{Lh}^*&I_{RL}\\I_{LR}&E_{Rh}^*\end{bmatrix}\begin{bmatrix}c_L^*\\c_R^*\end{bmatrix}=E_h\begin{bmatrix}c_L^*\\c_R^*\end{bmatrix}, \tag{A15}$$

where we use the following notation:

$$E^*_{Lh}=\frac{1}{1-\rho_h^2}\left\{\int d\mathbf{r}\ \psi_{Lh}(\mathbf{r})\mathcal{H}_h\psi_{Lh}(\mathbf{r}) - \rho_h^2\int d\mathbf{r}\ \psi_{Lh}(\mathbf{r})\mathcal{H}_h\psi_{Rh}(\mathbf{r})\right\}\approx E_{Lh}-\frac{\rho_h^2 b_{Lh}}{1-\rho_h^2}, \tag{A16}$$

$$E^*_{Rh}=\frac{1}{1-\rho_h^2}\left\{\int d\mathbf{r}\ \psi_{Rh}(\mathbf{r})\mathcal{H}_h\psi_{Rh}(\mathbf{r}) - \rho_h^2\int d\mathbf{r}\ \psi_{Rh}(\mathbf{r})\mathcal{H}_h\psi_{Lh}(\mathbf{r})\right\}\approx E_{Rh}-\frac{\rho_h^2 b_{Rh}}{1-\rho_h^2}, \tag{A17}$$

$$I_{LR}=\frac{1}{1-\rho_h^2}\left\{\int d\mathbf{r}\ \psi_{Rh}(\mathbf{r})\mathcal{H}_h\psi_{Lh}(\mathbf{r}) - \rho_h^2\int d\mathbf{r}\ \psi_{Lh}(\mathbf{r})\mathcal{H}_h\psi_{Lh}(\mathbf{r})\right\}\approx \frac{\rho_h b_{Lh}}{1-\rho_h^2}, \tag{A18}$$

$$I_{RL}=\frac{1}{1-\rho_h^2}\left\{\int d\mathbf{r}\ \psi_{Lh}(\mathbf{r})\mathcal{H}_h\psi_{Rh}(\mathbf{r}) - \rho_h^2\int d\mathbf{r}\ \psi_{Rh}(\mathbf{r})\mathcal{H}_h\psi_{Rh}(\mathbf{r})\right\}\approx \frac{\rho_h b_{Rh}}{1-\rho_h^2}, \tag{A19}$$

where

$$b_{Lh}=U_h\left(r_{Rh}\frac{\sigma_R^2}{\sigma_L^2+\sigma_R^2}\right)-U_{Lh}-\frac{1}{2}\hbar\omega_{0e}\left(\frac{\mu_h\omega_{Lh}^2}{\mu_e\omega_{0e}^2}\right)\times\left(\frac{r_{Rh}}{\lambda_{0e}}\frac{\sigma_R^2}{\sigma_L^2+\sigma_R^2}\right)^2, \tag{A20}$$

$$b_{Rh}=U_h\left(r_{Rh}\frac{\sigma_R^2}{\sigma_L^2+\sigma_R^2}\right)-U_{Rh}-\frac{1}{2}\hbar\omega_{0e}\left(\frac{\mu_h\omega_{Rh}^2}{\mu_e\omega_{0e}^2}\right)\times\left(\frac{r_{Rh}}{\lambda_{0e}}\frac{\sigma_R^2}{\sigma_L^2+\sigma_R^2}\right)^2. \tag{A21}$$

The overlap integral ρ_h can be evaluated using the saddle-point method, and reads

$$\rho_h=\beta\ \exp\left\{-\frac{r_{Rh}^2}{\lambda_{0e}^2}\frac{\sigma_R^2\sigma_L^2}{\sigma_R^2+\sigma_L^2}-\left[f_h\left(\frac{r_{Rh}}{\lambda_{0e}}\frac{\sigma_R^3}{\sigma_R^2+\sigma_L^2}\right) - f_h\left(\frac{r_{Rh}}{\lambda_{0e}}\sigma_R\right)\right]\right\}, \tag{A22}$$

where the prefactor β has the form

$$\beta=2\frac{\sigma_L}{\sigma_R}\left\{\frac{\sigma_R^2}{\sigma_R^2+\sigma_L^2}\exp\left[-\frac{r_{Rh}^2}{2\lambda_{0e}^2}\frac{\sigma_R^4}{\sigma_R^2+\sigma_L^2}\right] + \frac{r_{Rh}}{\lambda_{0e}}\frac{\sigma_R^3}{\sigma_R^2+\sigma_L^2}\sqrt{\frac{\pi}{2}\frac{\sigma_R^2}{\sigma_R^2+\sigma_L^2}}\times\left[1+\Phi\left(\frac{r_{Rh}}{\lambda_{0e}}\frac{\sigma_R^2}{\sqrt{2(\sigma_R^2+\sigma_L^2)}}\right)\right]\right\}\left\{\exp\left[-\frac{r_{Rh}^2\sigma_R^2}{\lambda_{0e}^2}\right] + \sqrt{\pi}\sigma_R\frac{r_{Rh}}{\lambda_{0e}}\left[1+\Phi\left(\frac{r_{Rh}}{\lambda_{0e}}\sigma_R\right)\right]\right\}^{-1/2}. \tag{A23}$$

The secular equation associated with the eigensystem (A15) reads

$$\det\begin{vmatrix}E_{Lh}-E_h & I_{LR}\\ I_{RL} & E_{Rh}-E_h\end{vmatrix}=0, \tag{A24}$$

and (assuming that $E_{Lh}>E_{Rh}$) has the solutions

$$E_h^{(1)}=E_{Lh}+\gamma_h, \tag{A25}$$

$$E_h^{(2)}=E_{Rh}-\gamma_h, \tag{A26}$$

where

$$\gamma_h=\frac{E_{Lh}-E_{Rh}}{2}\left\{\sqrt{1+\frac{4\rho_h^2 b_{Lh}b_{Rh}}{(1-\rho_h^2)(E_{Lh}-E_{Rh})^2}}-1\right\}. \tag{A27}$$

For each of energies E_h, the coefficients c_L^* and c_R^* can be now found, and the coefficients c_L and c_R are obtained via transformation (A13).

Additionally, the energy of the Coulomb interaction between an electron in the zeroth-order ground state (10) and a hole in the state with a given pair of coefficients c_L and c_R, can be written as

$$V_C=-\frac{e^2}{\epsilon\lambda_{0e}}\sqrt{\pi\beta}\int d\mathbf{r}_h\ \exp\left[-\frac{\beta r_h^2}{2\lambda_{0e}^2}\right]I_0\left[\frac{\beta r_h^2}{2\lambda_{0e}^2}\right]\times|c_L\psi_{Lh}(\mathbf{r}_h)+c_R\psi_{Rh}(\mathbf{r}_h)|^2. \tag{A28}$$

The value of this integral can be approximated using the saddle-point method:

$$V_C=-\frac{e^2}{\epsilon\lambda_{0e}}\sqrt{\pi\beta}\left\{c_L^2+c_R^2\ \exp\left[-\frac{\beta r_{Rh}^2}{2\lambda_{0e}^2}\right]I_0\left[\frac{\beta r_{Rh}^2}{2\lambda_{0e}^2}\right]+2c_Lc_R\times\exp\left[-\frac{\beta}{2}\left(\frac{r_{Rh}}{\lambda_{0e}}\frac{\sigma_R^2}{\sigma_L^2+\sigma_R^2}\right)^2\right]I_0\left[\frac{\beta}{2}\left(\frac{r_{Rh}}{\lambda_{0e}}\frac{\sigma_R^2}{\sigma_L^2+\sigma_R^2}\right)^2\right]\right\}. \tag{A29}$$

APPENDIX B

The Hartree potential of an electron in the presence of a hole is defined by Eq. (5). For the hole state in form (12), with a given pair of coefficients c_L and c_R, the interaction term in expression (5) can be written as

$$W(r)\equiv-\frac{e^2}{\epsilon}\int d\mathbf{r}'\frac{|\phi_h(\mathbf{r}')|^2}{|\mathbf{r}-\mathbf{r}'|} = c_L^2W_L(r)+c_R^2W_R(r)+2c_Lc_RW_{LR}(r). \tag{B1}$$

The potentials W_L and W_R are the Hartree potentials in the presence of a hole occupying the left or right single-well state, respectively, and W_{LR} is the off-diagonal term:

$$W_L(r)=-\frac{e^2}{\epsilon}\int d\mathbf{r}'\,\frac{|\psi_{Lh}(\mathbf{r}')|^2}{|\mathbf{r}-\mathbf{r}'|}=-\frac{e^2}{\epsilon\lambda_{0e}}A_{Lh}^2\int d\mathbf{x}\,\frac{\exp(-\sigma_L^2x'^2)}{|\mathbf{x}-\mathbf{x}'|}=-\frac{e^2}{\epsilon\lambda_{0e}}\sqrt{\pi}\sigma_L\,\exp\left(-\frac{\sigma_L^2x^2}{2\lambda_{0e}^2}\right)I_0\left(\frac{\sigma_L^2x^2}{2\lambda_{0e}^2}\right), \quad \text{(B2)}$$

$$W_R(r)=-\frac{e^2}{\epsilon}\int d\mathbf{r}'\,\frac{|\psi_{Rh}(\mathbf{r}')|^2}{|\mathbf{r}-\mathbf{r}'|}=-\frac{e^2}{\epsilon\lambda_{0e}}A_{Rh}^2\int d\mathbf{x}'\frac{\exp[-\sigma_R^2(x'-x_{Rh})^2-2\,f_h(\sigma_Rx')]}{|\mathbf{x}-\mathbf{x}'|}, \quad \text{(B3)}$$

$$W_{LR}(r)=-\frac{e^2}{\epsilon}\int d\mathbf{r}'\,\frac{\psi_{Lh}(\mathbf{r}')\psi_{Rh}(\mathbf{r}')}{|\mathbf{r}-\mathbf{r}'|}=-\frac{e^2}{\epsilon\lambda_{0e}}A_{Lh}A_{Rh}\int d\mathbf{x}'\frac{\exp[-\sigma_L^2x'^2/2-\sigma_R^2(x'-x_{Rh})^2/2-f_h(\sigma_Rx')]}{|\mathbf{x}-\mathbf{x}'|}, \quad \text{(B4)}$$

where we use the dimensionless coordinates $\mathbf{x}=\mathbf{r}/\lambda_{0e}$, $\mathbf{x}'=\mathbf{r}'/\lambda_{0e}$, and $x_{Rh}=r_{Rh}/\lambda_{0e}$. The function W_R can be evaluated using the saddle-point method:

$$W_R(r)=-\frac{e^2}{\epsilon\lambda_{0e}}\frac{\sigma_R^2}{2\pi}\frac{2\exp[2\,f_h(\sigma_Rr_{Rh}/\lambda_{0e})]}{\exp[-\sigma_R^2r_{Rh}^2/\lambda_{0e}^2]+\sqrt{\pi}[1+\Phi(\sigma_Rr_{Rh}/\lambda_{0e})]\sigma_Rr_{Rh}/\lambda_{0e}}\int d\mathbf{x}'\,\frac{\exp[-\sigma_R^2(x'-x_{Rh})^2-2\,f_h(\sigma_Rx')]}{|\mathbf{x}-\mathbf{x}'|}$$

$$\approx-\frac{e^2}{\epsilon\lambda_{0e}}\frac{\sigma_R^2}{\pi}\frac{1}{\exp[-\sigma_R^2r_{Rh}^2/\lambda_{0e}^2]+\sqrt{\pi}[1+\Phi(\sigma_Rr_{Rh}/\lambda_{0e})]\sigma_Rr_{Rh}/\lambda_{0e}}\int d\mathbf{x}'\,\frac{\exp[-\sigma_R^2(x'-x_{Rh})^2]}{|\mathbf{x}-\mathbf{x}'|}. \quad \text{(B5)}$$

We can see that, for $r\to\infty$,

$$W_R(r)\to-\frac{e^2}{\epsilon r}+O\left(\frac{1}{r^2}\right). \quad \text{(B6)}$$

Introducing the variable $\mathbf{x}''=\mathbf{x}'-\mathbf{x}$ from expression (B5), as follows:

$$\int d\mathbf{x}'\,\frac{\exp[-\sigma_R^2(x'-x_{Rh})^2]}{|\mathbf{x}-\mathbf{x}'|}=\exp[-\sigma_R^2(x^2+x_{Rh}^2)]\int_0^\infty dx''\exp[-\sigma_R^2x''^2]\int_0^{2\pi}d\theta\exp[-\sigma_R^2(2xx''\cos\theta$$

$$-2x_{Rh}\sqrt{x^2+x''^2+2xx''\cos\theta})]. \quad \text{(B7)}$$

The subintegral function reaches its maximum at $x''=0$. Therefore, at $x''/x\ll1$, we can use the expansion

$$\sqrt{x^2+x''^2+2xx''\cos\theta}=x\left[1+\frac{x''}{x}\cos\theta+\frac{1}{2}\left(\frac{x''}{x}\right)^2(1-\cos^2\theta)+\cdots\right]. \quad \text{(B8)}$$

We include only first two terms, i.e., we approximate the function W_R as follows:

$$W_R(r)=-2A\frac{e^2}{\epsilon\lambda_{0e}}\sigma_R^2\,\exp\left[-\left(\sigma_R\frac{r-r_{Rh}}{\lambda_{0e}}\right)^2\right]\int_0^\infty dx''\exp[-\sigma_R^2x''^2]\int_0^{2\pi}d\theta\exp[-2\sigma_R^2x''(x-x_{Rh})\cos\theta]$$

$$=-A\frac{e^2}{\epsilon\lambda_{0e}}\sigma_R\sqrt{\pi}\exp\left[-\frac{1}{2}\left(\sigma_R\frac{r-r_{Rh}}{\lambda_{0e}}\right)^2\right]I_0\left[\frac{1}{2}\left(\sigma_R\frac{r-r_{Rh}}{\lambda_{0e}}\right)^2\right], \quad \text{(B9)}$$

where

$$A=\frac{A'}{2\pi}\left\{\exp\left[-\frac{1}{2}\left(\sigma_R\frac{r-r_{Rh}}{\lambda_{0e}}\right)^2\right]+\sqrt{\pi}\sigma_R\frac{r_{Rh}}{\lambda_{0e}}\left[1+\Phi\left(\sigma_R\frac{r_{Rh}}{\lambda_{0e}}\right)\right]\right\}^{-1}. \quad \text{(B10)}$$

The constant factor A' was introduced in order to compensate for the rejection of multipliers in Eq. (B5). This factor ensures the proper asymptotical behavior of the function W_R for $r\to\infty$. Because expression (B9) for $r\to\infty$ takes the form

$$W_R(r)\to-\frac{e^2}{\epsilon r}A+O\left(\frac{1}{r^2}\right), \quad \text{(B11)}$$

then the consistence with Eq. (B6) requires the choice of A' such that $A=1$. This leads to the expression

$$W_R(r)=-\frac{e^2}{\epsilon\lambda_{0e}}\sigma_R\sqrt{\pi}\exp\left[-\frac{1}{2}\left(\sigma_R\frac{r-r_{Rh}}{\lambda_{0e}}\right)^2\right]I_0\left[\frac{1}{2}\left(\sigma_R\frac{r-r_{Rh}}{\lambda_{0e}}\right)^2\right]. \quad \text{(B12)}$$

We use further the same procedure to approximate the function W_{LR}:

$$W_{LR}(r)=-\frac{e^2}{\epsilon\lambda_{0e}}\sqrt{\pi}\rho_h\sqrt{\frac{\sigma_L^2+\sigma_R^2}{2}}\exp\left[-\frac{\sigma_L^2+\sigma_R^2}{4\lambda_{0e}^2}\left(r-\frac{r_{Rh}\sigma_R^2}{\sigma_L^2+\sigma_R^2}\right)^2\right]I_0\left[\frac{\sigma_L^2+\sigma_R^2}{4\lambda_{0e}^2}\left(r-\frac{r_{Rh}\sigma_R^2}{\sigma_L^2+\sigma_R^2}\right)^2\right]. \quad \text{(B13)}$$

Finally, the interaction part of the electron Hartree potential W takes the form

$$W(r)=-\sqrt{\pi}\,\frac{e^2}{\epsilon\lambda_{0e}}\left\{c_L^2\sigma_L^2\exp\left[-\frac{1}{2}\left(\sigma_L\frac{r}{\lambda_{0e}}\right)^2\right]I_0\left[\frac{1}{2}\left(\sigma_L\frac{r}{\lambda_{0e}}\right)^2\right]+c_R^2\sigma_R\exp\left[-\frac{1}{2}\left(\sigma_R\frac{r-r_{Rh}}{\lambda_{0e}}\right)^2\right]I_0\left[\frac{1}{2}\left(\sigma_R\frac{r-r_{Rh}}{\lambda_{0e}}\right)^2\right]\right.$$
$$\left.+2c_Lc_R\rho_h\sqrt{\frac{\sigma_L^2+\sigma_R^2}{2}}\exp\left[-\frac{\sigma_L^2+\sigma_R^2}{4\lambda_{0e}^2}\left(r-\frac{r_{Rh}\sigma_R^2}{\sigma_L^2+\sigma_R^2}\right)^2\right]I_0\left[\frac{\sigma_L^2+\sigma_R^2}{4\lambda_{0e}^2}\left(r-\frac{r_{Rh}\sigma_R^2}{\sigma_L^2+\sigma_R^2}\right)^2\right]\right\}. \quad \text{(B14)}$$

[1] For recent reviews and references, see T. Chakraborty, Comments Condens. Matter Phys. **16**, 35 (1992); M. Kastner, Phys. Today **46(1)**, 24 (1993); R. C. Ashoori, Nature (London) **379**, 413 (1996).

[2] L. Jacak, P. Hawrylak, and A. Wójs, *Quantum Dots* (Springer-Verlag, Berlin, 1997).

[3] T. Demel, D. Heitmann, P. Grambow, and K. Ploog, Phys. Rev. Lett. **64**, 788 (1990).

[4] R. C. Ashoori, H. L. Störmer, J. S. Weiner, L. N. Pfeiffer, K. W. Baldwin, and K. West, Phys. Rev. Lett. **71**, 613 (1993).

[5] B. Meurer, D. Heitmann, and K. Ploog, Phys. Rev. Lett. **68**, 1371 (1992).

[6] P. M. Petroff and S. P. DenBaars, Superlattices Microstruct. **15**, 15 (1994).

[7] S. Fafard, D. Leonard, J. L. Merz, and P. M. Petroff, Appl. Phys. Lett. **65**, 1388 (1994); S. Fafard, R. Leon, D. Leonard, J. L. Merz, and P. M. Petroff, Phys. Rev. B **52**, 5752 (1995).

[8] S. Fafard, K. Hinzer, S. Raymond, M. Dion, J. McCaffrey, Y. Feng, and S. Charbonneau, Science **274**, 1350 (1996).

[9] S. Raymond, P. Hawrylak, C. Gould, S. Fafard, A. Sachrajda, M. Potemski, A. Wójs, S. Charbonneau, D. Leonard, P. M. Petroff, and J. L. Merz, Solid State Commun. **101**, 883 (1997).

[10] N. Kirstaedter, N. N. Ledentsov, M. Grudmann, D. Bimberg, V. M. Ustinov, S. S. Ruvimov, N. V. Maximov, P. S. Kop'ev, Z. J. Alferov, V. Richter, P. Werner, V. Gösele, and J. Heydenreich, Electron. Lett. **30**, 1416 (1994).

[11] M. Grundmann, J. Christen, N. N. Ledentsov, J. Bohrer, D. Bimberg, S. S. Ruvimov, P. Werner, U. Richter, U. Gosele, J. Heydenreich, V. M. Ustinov, A. Yu. Egorov, A. E. Zhukov, P. S. Kop'ev, and Zh. I. Alferov, Phys. Rev. Lett. **74**, 4043 (1995); M. Grundmann, O. Stier, and D. Bimberg, Phys. Rev. B **52**, 11 969 (1995); M. Grundmann, N. N. Ledentsov, O. Stier, J. Böhrer, D. Bimberg, V. M. Ustinov, P. S. Kop'ev, and Zh. I. Alferov, *ibid.* **53**, R10 509 (1996).

[12] K. Brunner, U. Bockelmann, G. Abstreiter, W. Walther, G. Böhm, G. Tränkle, and G. Weimann, Phys. Rev. Lett. **69**, 3216 (1992).

[13] U. Bockelmann, K. Brunner, and G. Abstreiter, Solid-State Electron. **37**, 1109 (1994).

[14] M. Bayer, A. Schmidt, A. Forchel, F. Faller, T. L. Reinecke, P. A. Knipp, A. A. Dremin, and V. D. Kulakovskii, Phys. Rev. Lett. **74**, 3439 (1995).

[15] K. Imamura, Y. Sugiyama, Y. Nakata, S. Muto, and N. Yokoyama, Jpn. J. Appl. Phys. **34**, L1445 (1995).

[16] A. Wójs, P. Hawrylak, S. Fafard, and L. Jacak, Phys. Rev. B **54**, 5604 (1996); A. Wójs and P. Hawrylak, Solid State Commun. **100**, 487 (1996).

[17] A. Kumar, S. E. Laux, and F. Stern, Phys. Rev. B **42**, 5166 (1990).

[18] P. Vincente, A. Raymond, M. Kamal Saadi, B. Cousinet, M. Kubisa, W. Zawadzki, and B. Etienne, Solid State Commun. **96**, 901 (1995).